Turbulence, Heat and Mass Transfer 5, Sept. 25-29 2006, Dubrovnik
K. Hanjalic, Y. Nagano and S. Jakirlic (Editors)

Effects of Interfacial Velocity Boundary Condition on Turbulent Mass Transfer at High Schmidt Numbers

Y. Hasegawa and N. Kasagi
Department of Mechanical Engineering, The University of Tokyo, Hongo, Bunkyo-ku, Tokyo 113-8656, Japan, hasegawa@thtlab.t.u-tokyo.ac.jp, kasagi@thtlab.t.u-tokyo.ac.jp

Abstract - Numerical simulation of high Schmidt number turbulent mass transfer across free and solid surfaces is carried out. Near the free surface, the concentration field quickly responses to the normal velocity fluctuation and the eddy diffusivity is almost unchanged at a wide range of the Schmidt number. Whereas, near the solid wall, the concentration field becomes more insensitive to the normal velocity fluctuation and the eddy diffusivity is drastically decreased with increasing the Schmidt number. This fundamental difference between the concentration field close to the free and solid surfaces can be attributed to the difference of the spatial variation of the normal velocity fluctuation, namely, the normal velocity varies linearly with the distance from the free surface, while quadratically near the solid surface. The strong damping of the high-frequency concentration fluctuation near the solid surface agrees fairly well with the theoretical analysis by Shaw and Hanratty. These results indicate that the classical approach, which assumes the analogy between momentum and mass transfer near the solid wall, can not be used at the high Schmidt numbers.

1. Introduction

Heat and mass transfer across free and solid surfaces plays an important role in a variety of engineering applications. Considering the mass transfer inside liquid, the Schmidt number is commonly high ($Sc \sim O(10^3)$) and the transport mechanism is governed by turbulent motions within a thin concentration boundary layer ($\delta_c \sim O(10\ \mu\text{m})$).

In previous work [1], we investigated the microscopic mechanism of the mass transfer across clean and contaminated air-water interfaces. At the clean interface, the interfacial scalar flux quickly responses to the normal velocity fluctuation. With increasing the degree of surface contamination, however, the high-frequency concentration fluctuation is strongly damped and the mass transfer rate deteriorates and eventually falls down to the value on a solid wall. This fundamental difference between the concentration fields close to free and solid surfaces was first discussed by McCready and Hanratty [2]. They argued that v plays a critical role in the interfacial mass transfer, where v is the velocity component in the y direction and y is the distance from the interface. By expanding v in a Taylor series as $v(t,y) = \beta(t)y$ and $v(t,y) = \gamma(t)y^2$ at free and solid surfaces, respectively, they obtained the following relationships for high frequencies. For the free surface,

$$W_q(\omega) = \frac{W_\beta(\omega)}{\omega^2} Q^2, \tag{1}$$

whereas, for the solid surface [3],

$$W_q(\omega) = \frac{W_\gamma(\omega)}{Sc \cdot \omega^3} Q^2, \tag{2}$$

Here, W_q, W_β and W_γ are frequency spectra of the interfacial scalar flux q and the normal velocity fluctuations at the free and solid surfaces. The above equations imply the concentration fluctuation near the solid surface is damped faster than that near the free surface with increasing the frequency ω. Furthermore, appearance of Sc in the denominator of Eq. (2) reveals that the filtering near the solid surface is more enhanced at the higher Schmidt numbers.

This filtering effect has a strong impact on the limiting behavior of an eddy diffusivity E_c. Since the most change of mean concentration occurs in the viscous sublayer at the high Schmidt numbers, a Taylor series has been usually employed for representation of the velocity and concentration fields in the vicinity of the solid surface. In consideration of no-slip and constant concentration conditions, the eddy diffusivity can be expanded as follows:

$$E_c^+ = \frac{D^t}{\nu} = -\overline{c^{+\prime} v^{+\prime}} \left(\frac{dC^+}{dy^+} \right)^{-1} \sim A_3 y^{+3} + O\left(y^{+4}\right). \tag{3}$$

An eddy viscosity E_v is also given as:

$$E_v^+ = \frac{\nu^t}{\nu} = -\overline{u^{+\prime} v^{+\prime}} \left(\frac{dU^+}{dy^+} \right)^{-1} \sim B_3 y^{+3} + O\left(y^{+4}\right). \tag{4}$$

Since both the eddy diffusivity and the eddy viscosity vary as y^3 near the solid surface, the analogy between momentum and mass transfer, *i.e.*, $E_c = E_v$, has been widely used in engineering applications. This leads to the well-known relationship, namely, $K / u_\tau \propto Sc^{-2/3}$, where K is the mass transfer rate and u_τ is the friction velocity. According to precise experiments conducted by Shaw and Hanratty [4], however, K was proportional to $Sc^{-0.7}$. They also showed that the contribution of large wavenumbers to turbulent mass flux is strongly damped at the high Schmidt numbers. Numerical simulation by Na and Hanratty [5] showed that the coefficient A_3 in Eq. (3) decreases by about 30 % with increasing the Schmidt number from 1.0 to 10. These results suggest the breakdown of the analogy between momentum and mass transfer at the high Schmidt numbers. Hence, there has been strong need to investigate the limiting behavior of the concentration and velocity fields close to the solid surface. Although numerical simulation is useful to obtain detailed statistics inside the concentration boundary layer, most of the previous work is limited to the low to moderate Schmidt numbers ($Sc \sim O$ (10)).

In this work, we carry out numerical simulation of turbulent mass transfer at Sc = 100 across two distinct boundaries, *i.e.*, a clean air-water interface and a solid surface. Our main objective is to clarify the effects of the velocity boundary condition on turbulent mass transfer inside the viscous sublayer. Specifically, we examine the high Schmidt number effects on the limiting behavior of the eddy diffusivity and the damping of the concentration fluctuation close to the two boundaries.

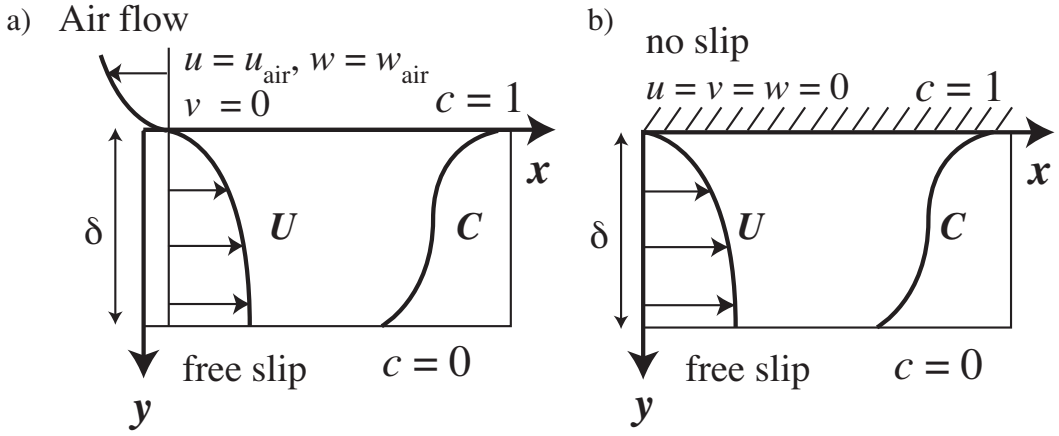

Fig. 1: Computational domain and coordinate system
a) Case 1: free surface, b) Case 2: solid surface

Table 1: Numerical scheme, number of modes and grid points, and grid spacings employed for calculation of the velocity and concentration fields

		Region	k_x, k_y or N_y, k_z	Δx_L^+	Δy_L^+	Δz_L^+
Velocity and Concentration (Sc = 1)	DNS	$0 < y_L^+ < 150$	64, 129, 64	18.4	0.01 ~ 1.23	7.2
Concentration (Sc = 100)	DNS	$0 < y_L^+ < 11.3$	192, 34, 192	6.1	0.01 ~ 0.62	2.4
	Buffer	$11.3 < y_L^+ < 21.6$	192, 15, 192	6.1	0.66 ~ 0.85	2.4
	LES	$21.6 < y_L^+ < 150$	64, 144, 64	18.4	0.86 ~ 1.23	7.2

2. Computational Model and Numerical Method

We consider two flow conditions as shown in Figs. 1 a) and b). The first (Case1) is a fully developed air-water counter flow driven by a constant pressure gradient (see, Fig. 1 a)). x and z are the streamwise and spanwise directions and y denotes the distance from the air-water interface. The computational periods were chosen to be $2.5\pi\delta$ and $\pi\delta$ in the x and z directions, respectively.

The governing equations in each phase are the incompressible Navier-Stokes, continuity, and scalar transport equations.

$$\frac{\partial u_i}{\partial t} + u_j \frac{\partial u_i}{\partial x_j} = -\frac{\partial p}{\partial x_i} + \frac{1}{Re_\tau} \frac{\partial^2 u_i}{\partial x_j \partial x_j} \tag{5}$$

$$\frac{\partial u_i}{\partial x_i} = 0 \tag{6}$$

$$\frac{\partial c}{\partial t} + u_j \frac{\partial c}{\partial x_j} = \frac{1}{Re_\tau \cdot Sc} \frac{\partial^2 c}{\partial x_j \partial x_j} \tag{7}$$

where, the velocity u_i and the coordinate x_i are non-dimensionalized by u_τ and δ in each phase. The non-dimensional parameters which characterize the velocity and concentration fields are the Reynolds number $Re_\tau = u_\tau \delta/\nu$ and the Schmidt number $Sc = \nu/D$, where u_τ , δ, ν and D are the interfacial friction velocity, the depth of computational domain, the kinematic viscosity and the molecular diffusivity of scalar, respectively. The Reynolds numbers based on u_τ and δ in the air and water phases were $Re_{\tau w} = Re_{\tau a} = 150$, which approximately corresponds to an air-water flow at a wind speed of 2 m/s at $y_a = \delta$ and δ of 4 cm under the standard condition. The subscript a and w represent values in the air and water phases, respectively. The density ratio of water and air is $\rho_w / \rho_a = 841$.

Since we focused on the fundamental difference between the slip and no-slip boundary conditions at free and solid surfaces in terms of the mass transfer, the interfacial deformation was neglected to avoid additional influence. Hence, the resultant velocity boundary condition at the air-water interface is the continuity of the horizontal velocity as well as the shear stress.

$$u_{i_w} = \sqrt{\frac{\rho_w}{\rho_a}} u_{i_a} \text{ (i = 1 and 3)} \tag{8}$$

$$u_{2_w} = u_{2_a} = 0 \tag{9}$$

$$\frac{1}{Re_{\tau_w}} \frac{\partial u_{i_w}}{\partial x_{2_w}} = \frac{1}{Re_{\tau_a}} \frac{\partial u_{i_a}}{\partial x_{2_a}} \text{(i = 1 and 3)} \tag{10}$$

Hereafter, we will focus on only the water phase and omit the subscript of w.

In the second case (Case 2), the air-water interface was replaced by a no-slip boundary as shown in Fig. 1 b). Hence, the interfacial boundary conditions are given as:

$$u_1 = u_2 = u_3 = 0 \tag{11}$$

In both Cases 1 and 2, a free-slip condition was used at the bottom boundary. For the concentration field, a constant concentration boundary condition $c = 1$ was imposed at the interfaces, while $c = 0$ at the bottom. The Schmidt number Sc was changed from 1.0 to 100 in the two cases. Direct numerical simulation (DNS) was applied to the velocity and concentration fields at Sc = 1.0 by using a pseudo-spectral method. 64 x 64 Fourier modes in the x and z directions and 129 Chebyshev polynomials in the y direction were used. For time integration, the second-order Adams-Bashforth and Crank-Nicolson schemes were adopted for the nonlinear and diffusion terms, respectively.

Since the concentration dissipation wave number, *i.e.*, the Batchelor wave number k_B, is generally proportional to $Sc^{1/2}$, $N^3 \propto Sc^{3/2}$ computation grids are required in order to resolve all essential scales of the concentration field. Meanwhile in the case of the interfacial mass transfer, most concentration change occurs in the vicinity of the interface. Therefore, in order to calculate the concentration field at Sc = 100, we employed a hybrid DNS/LES method [1], in which DNS with high-resolution grids, *i.e.*, $(k_x, N_y, k_z) = (192, 49, 192)$, is employed within a near-interface region $y^+ < 21.5$, while LES with coarser grids for the outer layer. Number of modes and grid points and grid spacings employed in each region are listed in Table 1. Details of the numerical scheme can be found in Hasegawa and Kasagi [1].

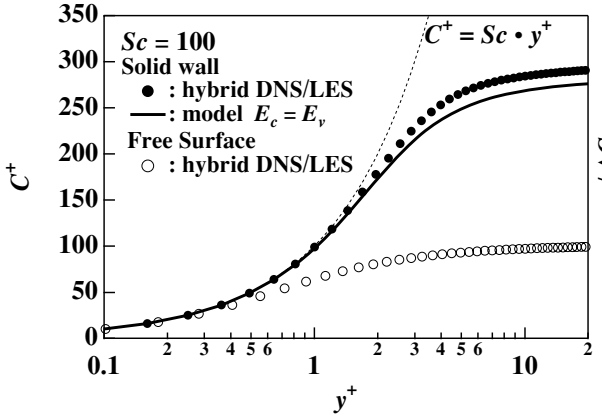

Fig. 2: Mean concentration profiles

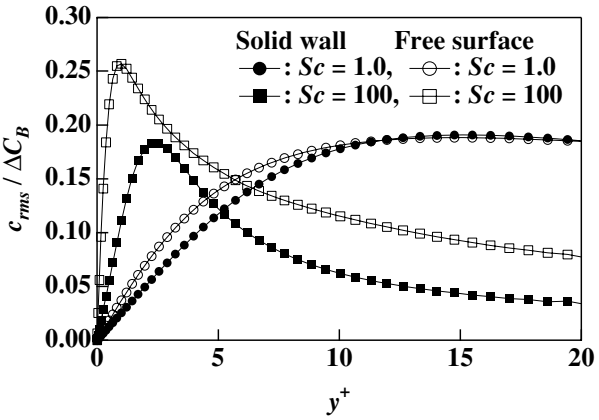

Fig. 3: Concentration fluctuations

The time increment was $\Delta t^+ = 0.018$ in all cases. In order to obtain statistics of the velocity and concentration fields, the time integration was repeated for $t^+ = 1000$ after the velocity and concentration fields reached the statistically stationary state.

3. Results

3. 1 Statistics of concentration field

The flow statistics under the present flow conditions have been already reported in our previous work [1]. The mean concentration profiles near the free and solid surfaces at $Sc = 100$ are presented in Fig. 2. The abscissa is the distance from the interface in the shear unit. The ordinate is the mean concentration relative to the interfacial concentration non-dimensionalized by the friction concentration. The conductive sublayer, in which $C^+ = Sc \cdot y^+$, exists in both cases. The thickness of the conductive sublayer is $\Delta^+_c = 0.24$ and 1.4 at the free and solid surfaces, respectively. The thinner conductive sublayer near the free surface indicates that turbulent eddies exist closer to the interface and enhance the mass transfer.

The concentration fluctuations, which are normalized by the difference, ΔC_B, of the interfacial concentration and the bulk concentration, are shown in Fig, 3. At $Sc = 1.0$, the profiles of c_{rms} near the free and solid surfaces are quite similar. Whereas at $Sc = 100$, the sharp maximum near the free surface is more prominent than that near the solid surface. With increasing the Schmidt number from 1.0 to 100, the peak location y^+_p approaches the interface, *i.e.*, from $y^+_p = 14.8$ to $y^+_p = 1.1$ and from $y^+_p = 15.5$ to $y^+_p = 2.5$ at the free and solid surfaces, respectively. These results suggest the free-surface turbulence penetrates the concentration boundary layer and effectively generates the concentration fluctuation.

Figures 4 a) and b) present the correlation coefficients $-R_{cu}$ and R_{cv} between the concentration and the streamwise and normal velocity fluctuations. Differences in $-R_{cu}$ and R_{cv} between the free and solid surfaces become apparent in the neighborhood of the boundary. At $Sc = 1.0$, $-R_{cu}$ is quite high ~ 0.9 near the solid surface due to similarity in the boundary conditions as well as the governing equations, namely, a no-slip condition $u' = 0$ and a constant concentration condition $c' = 0$ at the solid surface. With the Schmidt number increased, $-R_{cu}$ is decreased near both the free and solid surfaces (see, Fig. 4 a)). The interesting feature of the free surface is that R_{cv} is kept high ~ 0.6 even at the high Schmidt number (see, Fig. 4 b)). In contrast, near the solid

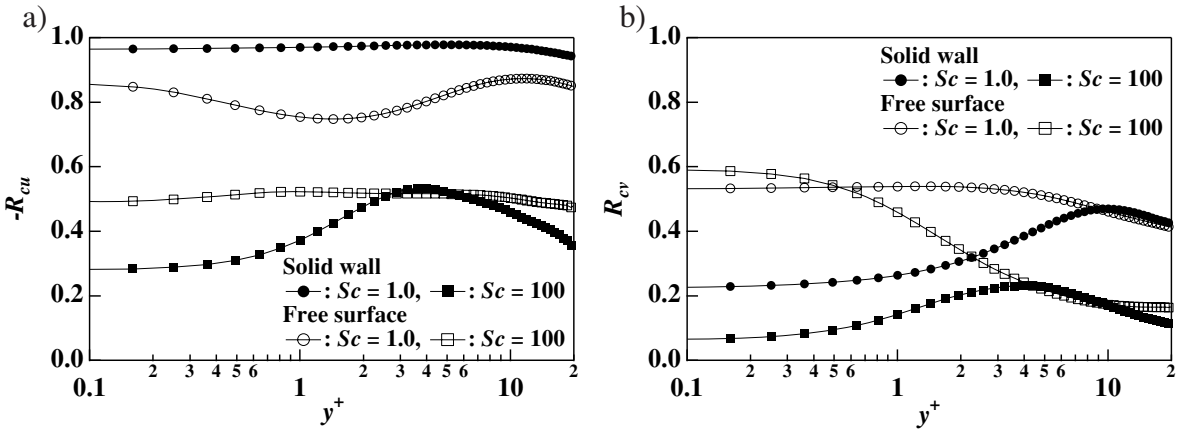

Fig. 4: Correlation coefficients a) $-R_{cu}$ and b) R_{cv}.

surface, R_{cv} is rapidly decreased with the Schmidt number increased.
These results indicate that the concentration field near the free surface quickly responds to the normal velocity fluctuation at a wide range of Schmidt numbers, whereas, near a solid surface, the concentration field becomes insensitive to the normal velocity fluctuations.

3. 2 Limiting behavior of eddy diffusivity near free and solid surfaces

Since the most concentration change occurs close to a surface at the high Schmidt numbers, the limiting behavior of the concentration and velocity fields is of particular importance for the modeling of mass transfer. Considering Eqs. (8-10) and a constant concentration condition at the free surface, the fluctuating velocity and concentration fields can be expanded in a Taylor series as follows:

$$c^{+\prime} = s_1 y^{+} + s_3 y^{+3} + O\left(y^{+4}\right), \tag{12}$$

$$u^{+\prime} = a_0 + a_1 y^{+} + O\left(y^{+2}\right), \tag{13}$$

$$v^{+\prime} = b_1 y^{+} + b_2 y^{+2} + O\left(y^{+3}\right). \tag{14}$$

Note that there is no y^2 term in the equation for c' because $\partial^2 c' / \partial y^2$ is identically zero at the isoconcentration boundary. The limiting expressions for the turbulent mass flux $\overline{c' v'}$ and the turbulent momentum flux $\overline{u' v'}$ in the y direction are also given as:

$$\overline{c^{+\prime} v^{+\prime}} = \overline{s_1 b_1} y^{+2} + \overline{s_1 b_2} y^{+3} + O\left(y^{+4}\right), \tag{15}$$

$$\overline{u^{+\prime} v^{+\prime}} = \overline{a_0 b_1} y^{+} + \overline{\left(a_0 b_2 + a_1 b_1\right)} y^{+2} + O\left(y^{+3}\right). \tag{16}$$

Similarly, considering no-slip and constant concentration conditions, the following expressions are obtained for the solid surface:

$$c^{+\prime} = s_1 y^{+} + s_3 y^{+3} + O\left(y^{+4}\right), \tag{17}$$

$$u^{+\prime} = a_1 y^{+} + a_2 y^{+2} + O\left(y^{+3}\right), \tag{18}$$

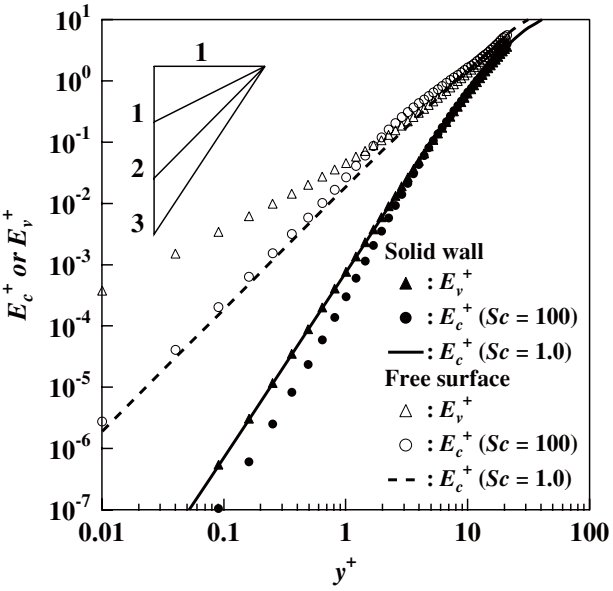

Fig. 5: Limiting behavior of eddy viscosity E_v^+ and eddy diffusivity E_c^+.

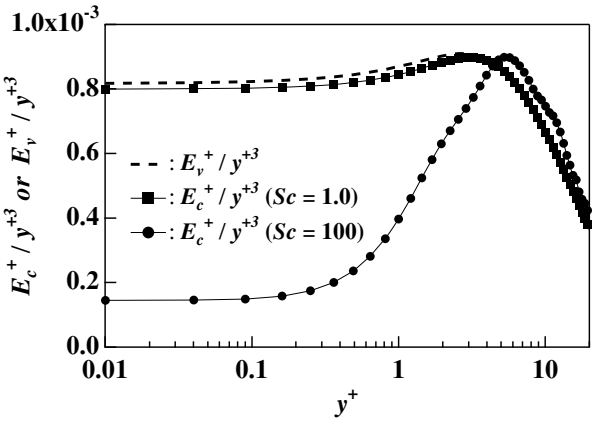

Fig. 6: Limiting behavior of E_v^+ / y^{+3} and E_c^+ / y^{+3} near the solid surface.

Table 2: Limiting values

	Sc = 1.0	Sc = 100
Free surface (A_2)	0.019	0.024
Solid surface (A_3)	0.00079	0.00014

$$v^{+\prime} = b_2 y^{+2} + b_3 y^{+3} + O\left(y^{+4}\right), \tag{19}$$

$$\overline{c^{+\prime} v^{+\prime}} = \overline{s_1 b_2} y^{+3} + \overline{s_1 b_3} y^{+4} + O\left(y^{+5}\right), \tag{20}$$

$$\overline{u^{+\prime} v^{+\prime}} = \overline{a_1 b_2} y^{+3} + \overline{\left(a_1 b_3 + a_2 b_2\right)} y^{+4} + O\left(y^{+5}\right). \tag{21}$$

The eddy diffusivity E_c^+ and the eddy viscosity E_v^+ are defined as:

$$E_c^+ = \overline{c^{+\prime} v^{+\prime}} \Big/ \left(\frac{\partial C^+}{\partial y^+}\right), \tag{22}$$

$$E_v^+ = -\overline{u^{+\prime} v^{+\prime}} \Big/ \left(\frac{\partial U^+}{\partial y^+}\right). \tag{23}$$

Since the mean concentration and the mean velocity can be expanded as $C^+ = 1 - Sc \cdot y^+ + O\left(y^{+2}\right)$ and $U^+ = y^+ + O\left(y^{+2}\right)$, respectively, the limiting behavior of E_c^+ and E_v^+ near the free surface is obtained from Eqs. (15) and (16) as:

$$E_c^+ = A_2 y^{+2} + O\left(y^{+3}\right), \tag{24}$$

$$E_v^+ = B_1 y^+ + O\left(y^{+2}\right), \tag{25}$$

where, $A_2 = \overline{s_1 b_1} / Sc$ and $B_1 = -\overline{a_0 b_1}$. Similarly, near the solid surface,

$$E_c^+ = A_3 y^{+3} + O\left(y^{+4}\right), \tag{26}$$

$$E_v^+ = B_3 y^{+3} + O\left(y^{+4}\right). \tag{27}$$

where, $A_3 = \overline{s_1 b_2} / Sc$ and $B_3 = -\overline{a_1 b_2}$.

In Fig. 5, the limiting behavior of E_c^+ and E_v^+ near the free and solid surfaces is plotted. Near the free surface, E_c^+ is almost independent of the Schmidt number. Near the solid surface, however, E_c^+ is drastically decreased with the Schmidt number increased. The limiting values of the eddy diffusivity, namely, A_2 and A_3 for the free and solid surfaces are listed in Table 2. The striking feature is that A_3 is decreased by about 80 % with the Schmidt number increased from 1.0 to 100. In order to look more closely, the limiting behavior of E_c^+ / y^{+3} and E_v^+ / y^{+3} near the solid surface is shown in Fig. 6. Due to Eqs. (26) and (27), the limiting values of E_c^+ / y^{+3} and E_v^+ / y^{+3} at the solid surface are identical to A_3 and B_3, respectively. At Sc = 1.0, E_c^+ agrees fairly well with E_v^+. In contrast, at Sc = 100, high Schmidt number effects clearly appear. In addition to the drastic decrease of the limiting value A_3, the thickness of the region where E_c^+ / y^{+3} is constant decreases with increasing the Schmidt number. This suggests that the assumption of $E_c^+ \propto y^{+3}$ is valid only in the conductive sublayer, where the contribution of turbulent transport is quite small compared with that of molecular transport. These results indicate that the analogy between momentum and mass transfer can not be used for prediction of the mass transfer at the high Schmidt numbers. A mean concentration profile calculated by assuming $E_c = E_v$ is plotted with a solid line in Fig. 2. A clear discrepancy with the hybrid DNS/LES data is confirmed.
In the following section, we examine the high Schmidt number effects in more detail by looking at frequency spectra of the concentration field close to the free and solid surfaces.

4. Frequency Spectra at High Schmidt Number

Because of the thin concentration boundary layer at the high Schmidt numbers, derivatives in the y direction are much larger that those in the other directions. Hence, the transport equation near an interface can be simplified as:

$$\frac{\partial c}{\partial t} + v\frac{\partial c}{\partial y} = \frac{1}{Sc}\frac{\partial^2 c}{\partial y^2}. \tag{28}$$

Here, all the variables are normalized by the shear units. A fundamental difference between a solid surface and a free surface is that the normal velocity fluctuation v varies quadratically with y near the solid surface, while linearly near the free surface. McCready and Hanratty [2] explored the effects of the limiting behavior of v on the sensitivity of the concentration boundary layer to high-frequency velocity fluctuation. By substituting $v = \gamma y^2 \cdot \exp(i\omega t)$ into Eq. (28), the following relationship was obtained for the solid surface:

$$W_q(\omega) = \frac{W_\gamma(\omega)}{Sc \cdot \omega^3} Q^2, \tag{29}$$

Similarly, for the free surface, substitution of $v = \beta y \cdot \exp(i\omega t)$ results in:

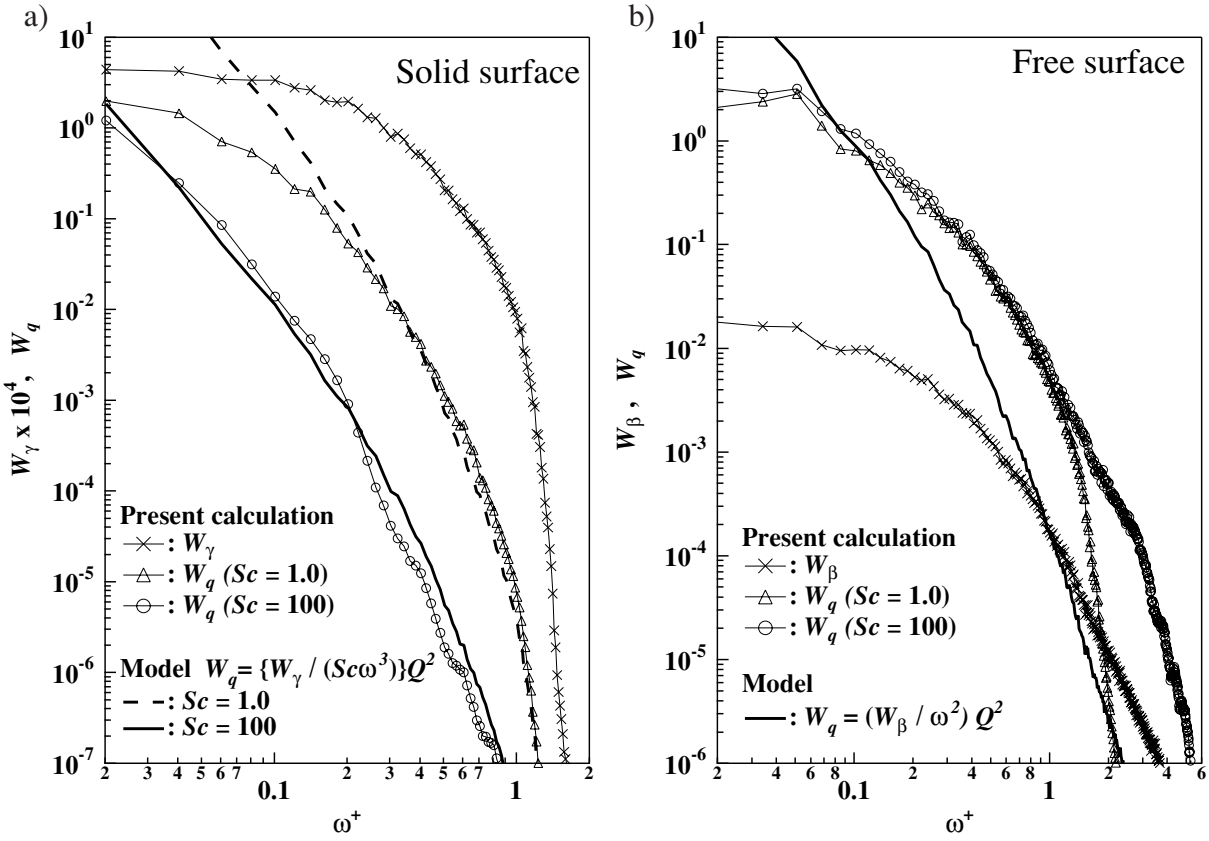

Fig. 7: Frequency spectra of interfacial mass flux q and normal velocity fluctuation at a) a solid surface and b) a free surface .

$$W_q(\omega) = \frac{W_\beta(\omega)}{\omega^2} Q^2, \tag{30}$$

where, W_q, W_γ and W_β are frequency spectra of the interfacial mass flux q, β and γ, respectively. Note that Eqs. (29) and (30) are valid only for high frequency, i.e., $Sc \cdot \omega >> 1$.

In Fig. 7 a) and b), W_q, W_γ and W_β at the solid and free surfaces are plotted. Excellent agreement between the present calculation and Eq. (29) is observed for the solid surface (see, Fig. 7 a)). The appearance of the Schmidt number in the denominator of Eq. (29) explains the strong damping of the concentration fluctuation at the high Schmidt number. In the case of the free surface, agreement between the present calculation and Eq. (30) is not so good as the case of the solid wall. Neglecting the convective terms in the x and z directions in Eq. (28) may cause this deviation, since the horizontal velocity components have non-negligible values at the free surface. It should be noted, however, that the damping of the concentration fluctuation is not observed at the free surface. This fact qualitatively coincides with Eq. (30), which is independent of the Schmidt number.

Frequency cospectra W_{cv} of the turbulent mass transport $c'v'$ in the y direction at $y^+ = 3.2$ from the solid and free surfaces are shown in Fig. 8 a) and b), respectively. Near the solid surface, the contribution of the high-frequency fluctuation on the turbulent mass transfer drastically decreases with increasing the Schmidt number. In contrast, near the free surface, the profile is

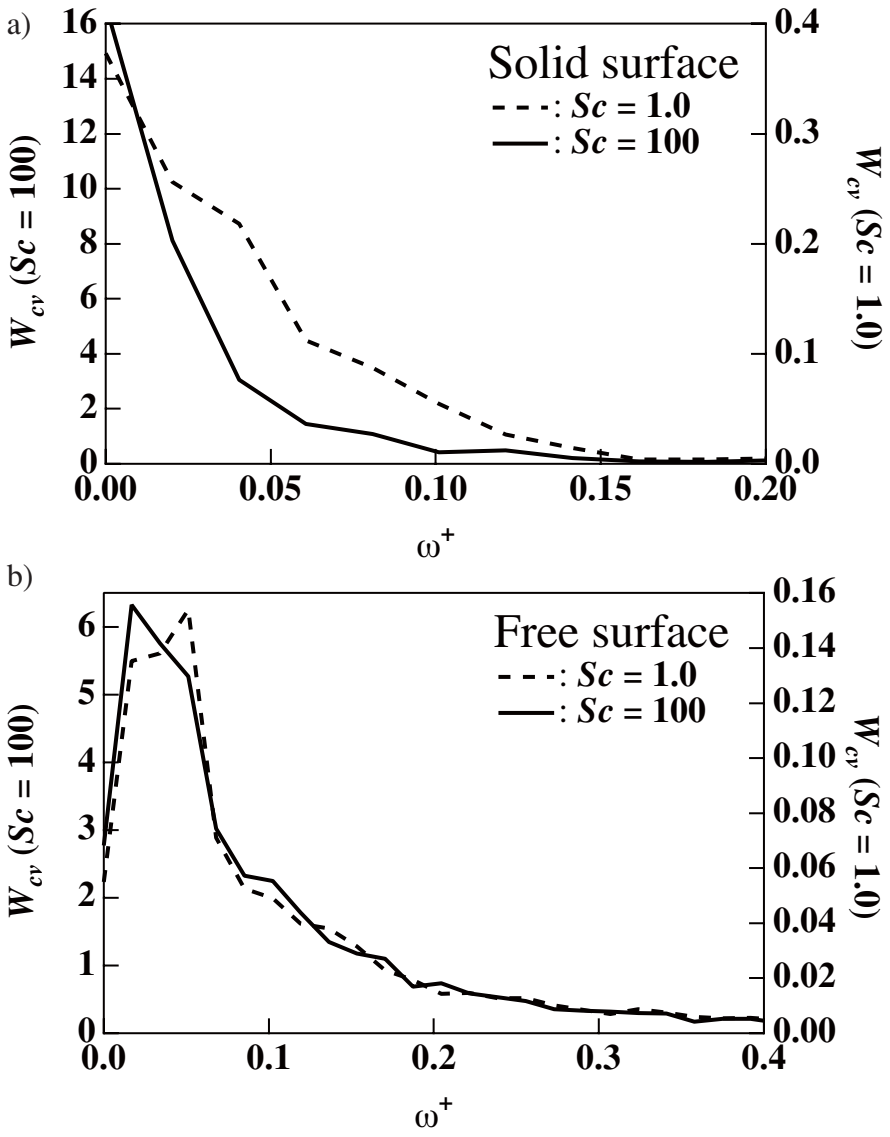

Fig. 8: Frequency cospectra of turbulent mass flux $c'v'$ at $y^+ = 3.2$
a): solid surface b): free surface

almost unchanged regardless of the Schmidt number. These results indicate that high-frequency velocity fluctuations play a more important role in the high Schmidt number mass transfer at the free surface than at the solid surface.

5. Conclusions

Distinct differences are observed between the concentration fields near free and solid surfaces at high Schmidt numbers. Near the free surface, the concentration field quickly responses to the normal velocity fluctuation and the limiting behavior of the eddy diffusivity is almost independent of the Schmidt number. On the other hand, near the solid surface, the concentration field becomes insensitive to the normal velocity fluctuation and the limiting value of the eddy diffusivity is decreased by around 80 % with the Schmidt number increased from 1.0 to 100.

At the high Schmidt numbers, almost all of the concentration change occurs in the near-wall

region, where $\nu^t \propto y^{+3}$. Hence, the assumption of $D^t \propto y^{+3}$ has been conventionally used within the whole concentration boundary layer. However, the present results show that the thickness of the region where $D^t \propto y^{+3}$ is decreased with increasing the Schmidt number and the region lies in the conductive sublayer where the turbulent transport is not significant. These results suggest that the analogy between momentum and mass transfer near the solid surface can not be used at the high Schmidt numbers.

These fundamental differences between the concentration filed near the free surface and that near the solid surface can be attributed to the difference of the spatial variation of the normal velocity fluctuation near the surfaces. According to the theoretical analysis of a one-dimensional advection-diffusion equation by McCready and Hanratty [2], it was shown that near the free surface, where the normal velocity varies linearly with y, the frequency spectrum of the concentration fluctuation is independent of the Schmidt number. This qualitatively agrees with the present result. In contrast, near the solid surface, where the normal velocity varies quadratically with y, similar analysis [3] revealed that the high-frequency concentration fluctuation is strongly damped with increasing the Schmidt number. The present result shows quantitative agreement with the theoretical prediction. Due to this low pass filtering effect, the contribution of the high-frequency velocity fluctuations to turbulent mass transport drastically decreases near the solid wall. This is the primary reason for the breakdown of the analogy between momentum and mass transfer. If we assume that the profile of the eddy diffusivity is unchanged from the present result even at higher Schmidt numbers, prediction by assuming $E_c = E_v$ overestimates the mass transfer rate 5 %, 15% and 40% at Sc = 100, 1000 and 1000, respectively. These results suggests that the filtering effect near the solid surface should be properly taken into account in order to predict the mass transfer rate at the high Schmidt numbers.

Acknowledgement

The present work was supported through the 21st Century COE Program, “Mechanical Systems Innovation,“ by the Ministry of Education, Culture, Sports, Science and Technology.

References

[1] Y. Hasegawa and N. Kasagi. Turbulent Mass Transfer Mechanism across a Contaminated Air-Water Interface. In *Fourth International Symposium on Turbulent Shear Flow Phenomena (Edited by J. A. C. Humphery, T. B. Gatski, J. K. Eaton, F. Friedrich, N. Kasagi, M. A. Leschzaner)*, pp. 971-976, 2005.

[2] M. J. McCready and T. J. Hanratty. Concentration Fluctuations close to a Gas-Liquid Interface. *AIChE Journal*, 30-5: 816-817, 1984.

[3] D. A. Shaw and T. J. Hanratty. Influence of Schmidt Number on the Fluctuations of Turbulent Mass Transfer to a Wall. *AIChE Journal*, 23-2: 160-169, 1977.

[4] D. A. Shaw and T. J. Hanratty. Turbulent Mass Transfer Rates to a Wall for Large Schmidt Number. *AIChE Journal*, 23-1: 28-37, 1977.

[5] Y. Na and T. J. Hanratty. Limiting Behavior of Turbulent Scalar Transport Close to a Wall. *Int. J. Heat and Mass Transfer*, 43: 1749-1758, 2000.